

## Computational Study of Interstitial Hydrogen Atoms in Nano-Diamond Grains Embedded in an Amorphous Carbon Shell

Amihai Silverman<sup>1</sup>, Alon Hoffman<sup>2</sup> and Joan Adler<sup>3,\*</sup>

<sup>1</sup> *Taub Computer Center, Technion-IIT, Haifa 32000, Israel.*

<sup>2</sup> *Schulich Faculty of Chemistry, Technion-IIT, Haifa 32000, Israel.*

<sup>3</sup> *Department of Physics, Technion-IIT, Haifa 32000, Israel.*

Received 27 January 2010; Accepted (in revised version) 29 June 2010

Available online 13 October 2010

---

**Abstract.** The properties of hydrogen atoms in a nano-diamond grain surrounded by an amorphous carbon shell are studied with Tight Binding computer simulations. Our samples model nano-diamond grains, of a few nanometers in size, that nucleate within an amorphous carbon matrix, as observed in deposition from a hydrocarbon rich plasma. The calculations show that the average hydrogen interstitial formation energy in the amorphous region is lower than in the nano-diamond core, therefore hydrogen interstitial sites in the in the amorphous region are more stable than in the nano-diamond core. This formation energy difference is the driving force for the diffusion of hydrogen atoms from nano-diamond grains into amorphous carbon regions. An energy well was observed on the amorphous side of the nano-diamond amorphous carbon interface: hydrogen atoms are expected to be trapped here. This scenario agrees with experimental results which show that hydrogen retention of diamond films increases with decreasing grain size, and suggest that hydrogen is bonded and trapped in nano-diamond grain boundaries and on internal grain surfaces.

**PACS:** 68.55.Ln, 71.15.Pd, 79.20.Uv, 81.05.Uw, 81.15.Gh

**Key words:** Nano-diamond, amorphous-carbon, DOS, NEXAFS, molecular-dynamics, tight-binding.

---

## 1 Introduction

Hydrogen is an essential component of the gas mixture used for micro and nano crystalline diamond film nucleation and growth by Chemical Vapor Deposition (CVD) methods [1–3]. Extensive research has been carried out to determine the role of hydrogen in

---

\*Corresponding author. *Email address:* phr76ja@technion.ac.il (J. Adler)

this process. When such deposition is made with energetic species, hydrogen-rich carbon films with nano-diamond grains a few nanometers in size, embedded into an amorphous carbon matrix [4], are created. The deposition parameters and properties of this class of films were extensively investigated and it was found that their formation is accompanied by a large hydrogen retention which was postulated to decorate the diamond grain boundaries [5]. It was recently reported by us and others that hydrogen retention in diamond films increases with decreasing diamond grain size [6]. In addition to the postulated location of hydrogen in the grain boundaries, other possible hydrogen locations are within the diamond grains as interstitial sites, forming defect-H clusters in the grains, on the diamond surfaces, or in non-diamond constituents between the grains (e.g., when nano-diamond crystallites are embedded in an a-C/graphite matrix). Hydrogen is extremely important to all structural changes in carbon materials, for example see [7].

In order to provide answers to key questions surrounding the location and properties of the hydrogen sites in diamond films, we carried out computer simulations with Tight Binding Molecular Dynamics (TBMD) methods. We calculated and compared the properties and energies of hydrogen atom interstitial sites in simulated samples of diamond, amorphous carbon and in mixed samples with an interface between a nano-diamond grain and an amorphous carbon shell. In a TBMD simulation, the band structure energy and the many body forces are calculated directly by diagonalizing the one electron Hamiltonian matrix [8–10]. Since the method is less computationally intensive than Local Density Approximation (LDA) [11,12] calculations, it allows us to study larger systems of atoms. Thus we can include important structural configurations such as nano-diamond in an amorphous matrix, and thereby study the interface region between diamond and amorphous structures. TBMD has been shown in the literature to give reliable results for amorphous carbon and amorphous hydrogenated carbon provided the selected TB parameters and simulation regime are appropriate [13].

Starting from translationally invariant pure diamond, our calculations were carried out in two stages. First, preliminary samples were prepared, using simpler molecular dynamics methods with empirical potentials [14, 15], because relatively long run times are sometimes needed at this stage. A melt-quench process [16, 17] was used to prepare either amorphous carbon, or a nano-diamond core surrounded by an amorphous carbon matrix. For the latter, some diamond sites were pinned during the melt-quench process to imitate a nano-diamond grain embedded into an amorphous carbon matrix after the nucleation process which was observed in the experiment [4]. Smaller samples, some with inverse structures of amorphous cores and crystalline surroundings, and others with melted stripes were previously generated in our group with this approach [18]. Mixed sample have also been prepared and investigated more recently by Kopidakis et al. in [19], who embedded nanocrystals in an amorphous matrix. We will return to a comparison with these below. Once the preliminary samples were obtained, a TBMD simulation using the Frauenheim's Tight Binding (FTB) model [8,10] was applied for both the C-H and C-C interactions to stabilize the sample, and obtain more accurate atomic configurations. In all cases, the initial sample was translationally invariant pure diamond.

After the two stage preparation process was completed, hydrogen atoms were inserted into the sample interiors and optimization techniques using the FTB model [8, 10] were applied to calculate the atomic configuration at the local-minimum in energy. The same process was performed for a large number of samples of the three types (diamond, amorphous and mixed); in each case one hydrogen atom was placed at a different interstitial site. The calculated hydrogen interstitial formation energies were plotted versus the distance from the interface between the diamond and the amorphous carbon. A preliminary version of some of the hydrogen interstitial results was given in [20]. For comparison purposes we also calculated the hydrogen atom formation energy in a pure diamond core for different hydrogen concentrations.

In the following sections we first describe the sample preparation in detail, and then present the results of our simulations with and without hydrogen. Then, we discuss these results in the light of the experimental measurements of hydrogen retention in diamond films carried out at the Technion.

## 2 Simulation samples and methods

Our samples consisted of 512 carbon atoms in a (100) cubic cell with periodic boundary conditions, and were initially in a pure diamond structure. Two different procedures were then used to prepare amorphous and mixed diamond/amorphous samples.

### 2.1 Amorphous carbon samples

The amorphous structures were obtained using a molecular dynamics melt-quench process [16, 17]. The Parrinello-Rahman [21, 22] NPT (fixed number of atoms  $N$ , pressure,  $P$ , and temperature  $T$ ) ensemble molecular dynamics algorithm was applied to melt the sample with all atoms free to move. Then, the sample was gradually cooled to allow the convergence of its volume, until equilibrium was obtained. The Stillinger-Weber [14] type empirical inter-atomic potentials, improved by Barnard-Russo [15] for tetrahedral carbon were used for the molecular dynamics inter-atomic force calculations at this initial melt-quench stage. Although such empirical inter-atomic potentials are less accurate than Tight Binding and Local Density Approximation (LDA) [11, 12], and can not access quantum mechanical phenomena such as bond breaking and recombination, they can successfully simulate the formation of an amorphous structure using a melt-quench process [16]. In fact they are the practical choice for the formation stage since other methods are too slow for simulating the long amorphous samples formation process for large samples with the required degree of equilibration. Careful annealing, with equilibrium at each temperature is essential for the development of stable amorphous structures in carbon [23].

At the end of the initial formation process, an additional, relatively long, molecular dynamics simulation using the Frauenheim's Tight Binding (FTB) model [8, 10] was applied to stabilize the sample, into even more accurate atomic configurations. These

calculations used the PLATO code [24,25]; with Conjugate Gradient (CG) algorithms [26] using the FTB model applied to obtain the final atomic configuration.

## 2.2 Mixed diamond/amorphous

The mixed samples consist of a nano-diamond core surrounded by a region of amorphous carbon. These samples were also obtained by a simulation of a melt-quench process [16, 17] of initial samples with a pure diamond structure, but 150 atoms in the core of the samples were pinned (i.e., not allowed to move) during the simulations [18]. After initial equilibration the same Parrinello-Rahman [22] NPT molecular dynamics algorithm was applied to the other 362 atoms followed again by a long molecular dynamics simulation using the FTB model to stabilize the sample.

## 2.3 Hydrogen interstitial sites

In the next stage, hydrogen atoms were inserted into interstitial sites of the three different sample types - diamond, amorphous and mixed. Then, hydrogen atoms were inserted into random locations in the samples, and Conjugate Gradient (CG) and Steepest Descent (SD) optimization methods [26] were used alternatively for the convergence of the atomic coordinates toward the local-minimum in energy using the FTB models [8, 10]. At this stage all the atoms were allowed to move, and at the end all the hydrogen atoms were located in interstitial sites. The mixed samples had only one hydrogen atom inserted, but multiple hydrogen atoms were inserted into the pure diamond sample and the amorphous samples for comparison purposes. The process of hydrogen interstitial site calculation was repeated roughly 100 times for different sites in the mixed samples, and roughly 30 times for different sites in the amorphous samples.

## 2.4 Sample integrity

For both the amorphous and mixed case, one may ask whether a particular sample is truly representative of the typical case. Apart from general checks such as comparison of Density of States (DOS) and Radial Distribution Functions (RDF) with other calculations, one way to explore this is to prepare several distinct samples and compare their characteristics. Four different amorphous samples and four different mixed samples were obtained by a melt-quench process using different time and temperature intervals during the formation process. We took great care with the annealing, and confirm that the sample characteristics were indeed reproducible.

## 2.5 Visualization

The atomic images in this article were drawn using AViz [27], and different greyscale values (color online) were used to indicate different atomic types.

### 3 Simulated samples-characteristics and comparison with NEXAFS

#### 3.1 NEXAFS compared to DOS calculations

The Near Edge X-ray Absorption Fine Structure (NEXAFS) [28] can be simulated from the electronic structure as calculated from computer simulations such as tight binding. Some initial steps towards such comparisons were made previously [29] and are developed more fully below. We find that these comparisons provide a powerful validation of the characteristics of our simulated samples, and together with comparisons with the Density of States (DOS) and Radial Distribution Functions (RDF) calculated by other groups [30–32] justify the physical basis of our computer simulation processes implemented for the generation of the amorphous carbon and mixed samples.

The NEXAFS spectrum near the core level excitation edge may be described to a first approximation by a summation over all optical transitions between the C(1s) and the un-occupied electronic states. Therefore it is expected that the NEXAFS intensity at each point in the energy scale will depend on the specific geometry determined by the sample surface crystallographic orientation, incident photon source and detector orientation. However, the NEXAFS spectrum of amorphous carbon is not expected to display this dependency since the selection rules “soften” or even break down the optical modes that are normally forbidden in the spectra of crystalline samples. These modes are therefore activated and contribute to the NEXAFS spectrum. Therefore a comparison between the NEXAFS and DOS near the excitation edge is justified for amorphous carbon, and one would expect both curves to display features at similar energies (with respect to the Fermi level) as was observed. More details on the comparisons for the amorphous situation are given below.

#### 3.2 Pure diamond

For the case of pure diamond the DOS/NEXAFS comparison may be less justifiable a priori since optical transition selection rules may have an important effect on the NEXAFS spectrum. Nevertheless, keeping this in mind, a general qualitative comparison may be made between the calculated DOS and the NEXAFS of diamond [28].

Our calculation for the DOS of our initial pure diamond sample, made with the FTB model [8], was compared with the NEXAFS of a pure diamond sample measured by us [33]. The NEXAFS measurements were carried out in the Partial Electron Yield (PEY) mode at SuperAco France using photon energies in the 285-320 eV range [33]. Fig. 1 shows the calculation of the DOS of a pure diamond sample above the Fermi level versus NEXAFS experimental results for a pure diamond sample. The NEXAFS plot was shifted along the  $X$  (energy) axis so that the first positive yield coincides with the Fermi level of the DOS calculation. From this figure a relatively good qualitative correspondence is observed between the features in the DOS and NEXAFS spectrum. An exception is the

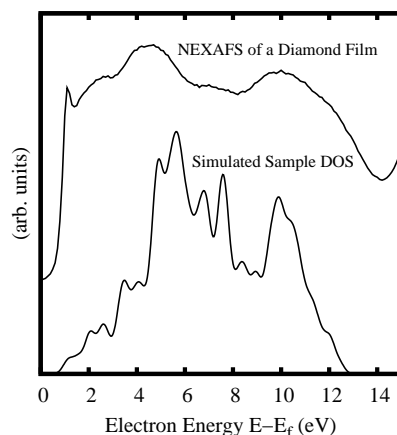


Figure 1: A Pure diamond simulated sample Density of States (DOS) above the Fermi level (lower plot) versus NEXAFS experimental results for a pure diamond film (upper plot).

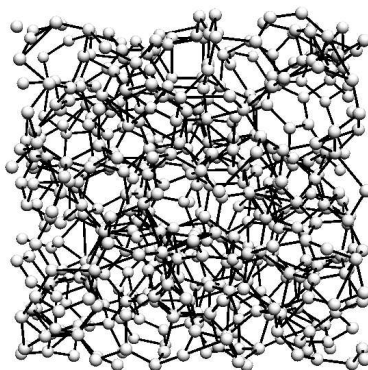


Figure 2: A view of the amorphous carbon sample.

sharp NEXAFS peak measured at  $\sim 1$  eV (full width at half maximum of 0.2 eV) which is associated with a bulk C(1s) exciton and therefore not expected to appear as a feature in the ground state DOS.

### 3.3 Amorphous carbon

An image of one of our amorphous samples, obtained from a simulated melt-quench process, (Section 2.1) is presented in Fig. 2 to aid the reader. Note that while the nearest neighbor distances are fairly similar, higher neighbor configurations and distances become quite irregular, and many atoms are three or two fold coordinated. Fig. 3 depicts the calculated RDF,  $g(r)$ , of the amorphous sample (lower plot) versus the calculated RDF of the amorphous carbon shell atoms in the mixed sample described in Section 3.4 (upper plot).

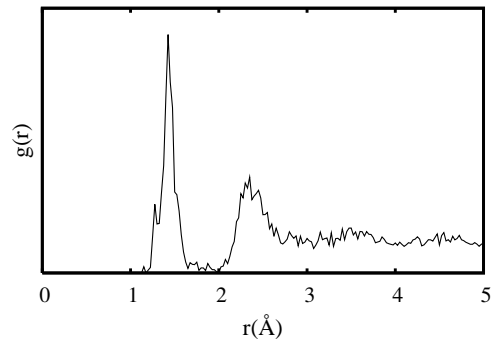


Figure 3: Radial Distribution Function (RDF) of the amorphous carbon shell atoms in the mixed sample (upper plot) and the RDF of an amorphous carbon sample (lower plot).

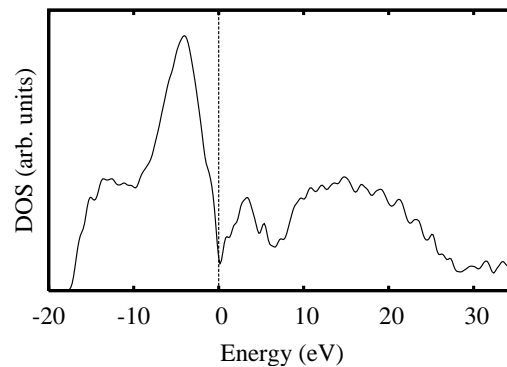


Figure 4: Electronic Density of States (DOS) of the simulated amorphous carbon sample. The zero of the energy is taken to be the Fermi level (denoted by the vertical line).

Fig. 4 shows the electronic DOS of the amorphous sample which was calculated using the FTB model [8]. The RDF and DOS results of our amorphous carbon samples are in agreement with other simulated samples of amorphous carbon obtained using different models for the inter-atomic interactions [30–32].

We compared the calculated DOS with the NEXAFS of an amorphous carbon film which were produced by in-situ 1000 eV Ar ion irradiation of a polycrystalline diamond film at a dose of  $\sim 5 \times 10^{15}$  ions/cm<sup>2</sup> [33]. Fig. 5 shows the simulated amorphous sample DOS above the Fermi level, compared with the NEXAFS of an amorphous carbon film [33]. The NEXAFS plot was shifted along the X (energy) axis so that the first positive yield coincides with the Fermi level of the DOS calculation.

As can be observed in Fig. 5, the calculated DOS above the Fermi level and the NEXAFS spectrum of the amorphous film display two peaks at very similar energies, 3 eV and 15 eV (with respect to the Fermi level). Considering that the NEXAFS spectrum in this energy range reflects the electronic DOS, the agreement between both spectra strongly confirm the validity of our amorphous carbon computational model.

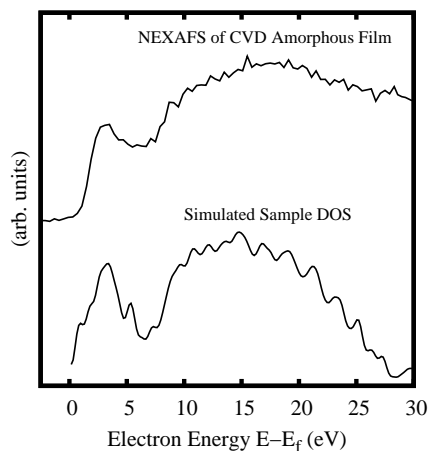


Figure 5: The amorphous carbon simulated sample Density of States (DOS) above the Fermi level (lower plot) versus NEXAFS experiment results of a CVD amorphous carbon film (upper plot). The resemblance justifies our amorphous model.

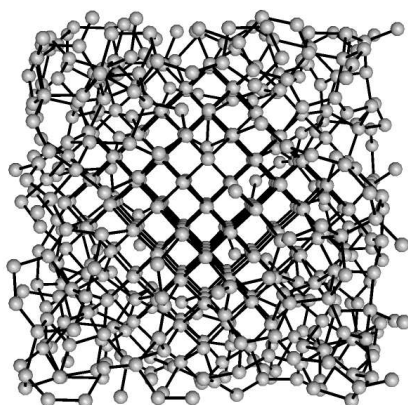


Figure 6: A view of the mixed sample-a nano-diamond core surrounded by amorphous carbon shell.

### 3.4 Mixed sample

In order to understand nano-diamond film formation from energetic species [4], simulated samples of a nano-diamond grain surrounded by an amorphous shell were prepared (see Section 2.2). Fig. 6 depicts an image of one of these mixed samples. Different time and temperature steps were used to form four different samples (as described above in Section 2.4). Fig. 7 shows the calculated DOS of the 362 shell atoms. This DOS agrees with that of Kopidakis et al. [19]. The Radial Distribution Function (RDF) calculated for the 362 shell atoms (not shown here, but similar to Fig. 3) revealed the characteristic pattern of an amorphous structure [17], confirming the amorphous nature of the shell atoms.

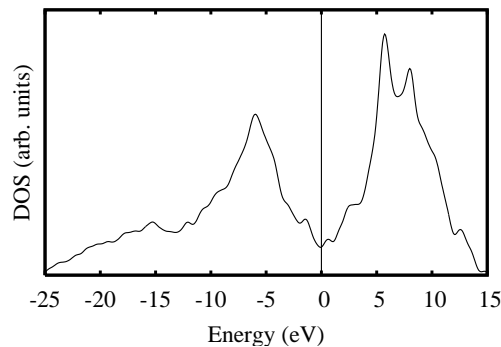


Figure 7: Electronic Density of States (DOS) of the amorphous atoms in the mixed sample. The zero of the energy is taken to be the Fermi level (denoted by the vertical line).

## 4 Hydrogen interstitial sites

In the following sections, we describe the behavior of our pure diamond, amorphous carbon and mixed samples when hydrogen atoms were inserted into interstitial sites.

### 4.1 Hydrogen interstitial sites in pure diamond

The structure and energy of hydrogen interstitial sites in pure diamond samples were calculated. This was carried out by inserting hydrogen atoms into random locations inside pure diamond samples, and relaxing the atomic configurations into the energy minimum. Two interstitial sites were observed, Bond-Centered (BC) and Tetrahedral (T) (in agreement with others [34–36]). We found an energy difference of 1.6 eV between the hydrogen interstitial sites at BC and T, compared to 1.7 eV in [34], and similarly in [37] and distinct from 1.17 eV in [35] and other DFT studies [38, 39]. An extensive discussion of this discrepancy was given in [34], including comparisons with [40].

The addition of a single hydrogen interstitial into pure diamond means a defect is formed and therefore the system energy is increased. For example, at a BC site, the hydrogen atom inserts itself into a C-C bond resulting in a stretched C-C bond. Adding another hydrogen interstitial near the one already present forms an Anti-Bonding (AB) site, which results in a decrease in the binding energy per hydrogen atom, thereby decreasing the interstitial formation energy per atom [42].

We observed that when further hydrogen atoms were added into pure diamond and the density was allowed to relax, the hydrogen interstitial formation energy was reduced significantly (i) as the hydrogen concentration increased, and (ii) as the sample density decreased. These effects are additive as increasing the hydrogen concentration increases the sample volume, and therefore reduces the density of the carbon atoms.

In order to check this systematically, a number of hydrogen atoms were gradually inserted into random sites in an initially pure diamond sample, and the energy was

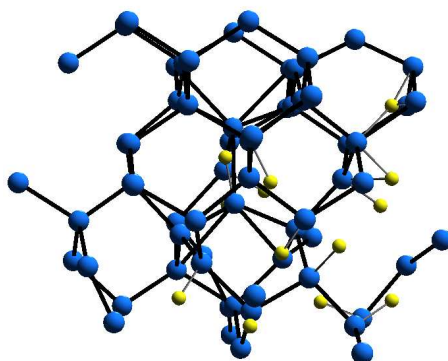


Figure 8: (Color online) A view of a portion of an initial pure diamond after 20 at.% hydrogen atoms were inserted. The large spheres (blue online) depict carbon atoms and the small spheres (yellow online) depict hydrogen atoms.

calculated after relaxation. After each insertion the Steepest Descent (SD) optimization method [26] was used to map the atomic configuration into the minimum energy configuration, then the density of the sample was mapped to the minimum energy density, and the energy of the sample  $E_{H_n}$  was calculated. All the energies were calculated using the FTB model [8] with periodic boundary conditions. A view of a portion of a sample with several hydrogens inserted is shown in Fig. 8. Larger aggregates, which superficially resemble parts of the structures in this figure were previously examined in [41].

In Fig. 9 the hydrogen interstitial formation energy per hydrogen atom  $E_{H_n}(i)$  is plotted as a function of the hydrogen concentration, where

$$E_{H_n}(i) = \frac{E_{H_n} - E_x - E_H(\text{vac})}{n}.$$

$E_{H_n}$  is the energy of the sample with  $n$  hydrogen atoms at interstitial sites,  $E_x$  is the energy of the initial pure diamond sample, and  $E_H(\text{vac}) = -5.44$  eV is the FTB energy of a hydrogen atom in vacuum, introduced as a reference point. This is in agreement with the incremental binding energy decreasing from 5.3 eV for the first to 2.5 eV for the fourth hydrogen interstitial atom calculated using semi-empirical cluster methods [42], and with 5.1 eV calculated for the energy of the most stable hydrogen site in diamond using a Hartree-Fock approximation with the method of partial retention of diatomic differential overlap [43].

We observe that the average hydrogen interstitial formation energy decreases with increasing hydrogen concentration. This behavior is explained as follows: after inserting hydrogen atoms into a pure diamond sample, the volume is increased and defects and dangling bonds are formed. When more hydrogen atoms are inserted, they enter into defect sites, terminate dangling bonds and therefore reduce the system energy. The higher the hydrogen concentration, the more defects are formed.

From Fig. 9 we also observe that the hydrogen interstitial formation energy is positive when the hydrogen concentration is below 20 at.%, and negative elsewhere. Therefore,

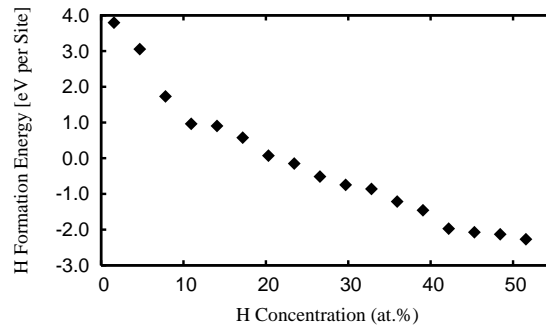


Figure 9: The average hydrogen interstitial formation energy in an initial pure diamond with hydrogen interstitial sites, as a function of hydrogen concentration.

inserting a low concentration of hydrogen into a pure diamond increases the system energy, but once the hydrogen concentration rises above some 20 at.%, inserting additional hydrogen atoms decreases the system energy.

## 4.2 Hydrogen interstitial sites in amorphous carbon

Different interstitial site locations for hydrogen were examined for different simulated amorphous carbon samples, and the hydrogen interstitial formation energies  $E_H(i)$  for different hydrogen interstitial sites were calculated as  $E_H(i) = E_H - E_x - E_H(\text{vac})$ , where  $E_H$  is the energy of the sample with a hydrogen atom at an interstitial site,  $E_x$  is the energy of the initial amorphous carbon sample (without the hydrogen atom) and  $E_H(\text{vac})$  is the energy of a hydrogen atom in vacuum (all energies were calculated using the FTB model [8]). On averaging  $E_H(i)$  over different amorphous carbon samples and different hydrogen sites we found  $E_H(i)_{\text{av}} = -5.2 \pm 1.5$  eV. The FTB model C-H bond energy is  $E_{\text{C-H}} = -5.48$  eV, within the range of  $E_H(i)_{\text{av}}$ , therefore we deduce that hydrogen atoms which were inserted into the amorphous carbon matrix were bonded to carbon atoms, terminating dangling bonds. Dangling bonds are widespread in amorphous carbon due to the disordered nature of the system where many carbon atoms are three-fold coordinated [44,45].

We also calculated the interstitial hydrogen formation energy in amorphous carbon samples with different hydrogen concentrations. The average hydrogen interstitial formation energies (averaged over different samples and different sites) fell within the same range for different hydrogen concentrations. Unlike the situation in pure diamond where the hydrogen interstitial sites form defects and therefore the energy per hydrogen interstitial site decreases with hydrogen concentration, in amorphous carbon, the hydrogen atoms do not create new defects, but are bonded to dangling bonds in existing defects, and therefore the energy per hydrogen interstitial site remains within the same range as the hydrogen concentration increases [44,45].

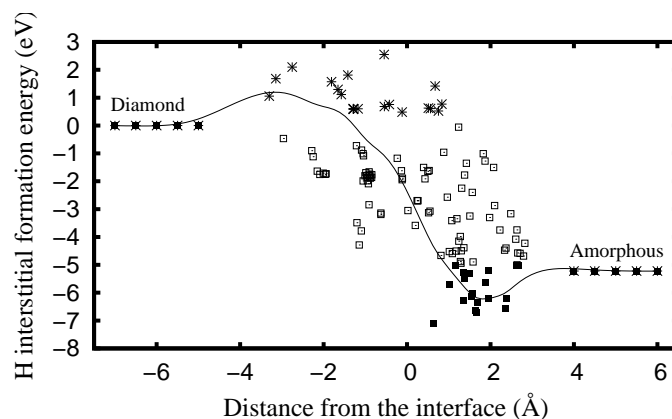


Figure 10: The hydrogen interstitial formation energy  $E_H(i)$  for different radial distances from the interface at  $x=0$  between the crystalline and amorphous regions. Each point represents a different hydrogen interstitial site. The asterisks represent hydrogen sites with positive energy, the squares represent hydrogen sites which decrease the system energy, and the filled squares represent the cases where the interstitial energy is lower than the interstitial energy in the amorphous carbon region. The continuous line depicts a cubic spline interpolation to guide the eye.

### 4.3 Hydrogen interstitial sites in the mixed samples

After the simulations with multiple H atoms described above were carried out we next inserted single hydrogen atoms into different interstitial sites of the mixed samples. The crystalline core of the sample has an almost spherical shape with radial symmetry (see Fig. 6), and therefore the interface between the crystalline core atoms and the amorphous layer is at the same radial distance from the center of the sample. The radial distance of each interstitial site from the center of the sample was calculated, and plotted versus the interstitial site energy. The hydrogen interstitial site energy was calculated in the same way as in the previous section from  $E_H(i) = E_H - E_x - E_H(\text{vac})$  except that here  $E_H$  is the energy of the mixed sample with the hydrogen atom in an interstitial site,  $E_x$  is the energy of the initial mixed sample without the hydrogen atom and  $E_H(\text{vac})$  is the energy of a hydrogen atom in vacuum (calculated using the FTB model [8]).

In Fig. 10 the hydrogen interstitial energy  $E_H(i)$  is plotted for various interstitial sites. The X axis is the radial distance of the hydrogen atom interstitial from the interface between the crystalline and amorphous regions, with the interface at  $X=0$ . Each point in the plot represents a different interstitial site. The five points on the left-hand-side of the plot represent the average hydrogen site formation energy in pure diamond, as reported in Section 4.1 (Fig. 9) for hydrogen concentration of 19 at.%. This concentration is that measured by us in nano-diamond films [5]. The five points on the right-hand-side represent the average hydrogen site formation energy in amorphous carbon (see Section 4.2).

Three different cases of interstitial sites were catalogued in the interface region. (i) Sites with positive energy where the hydrogen atom creates a defect in the structure

(similar to the case of hydrogen sites in pure diamond), and therefore increases the systems energy, indicated by asterisks in the figure. (ii) Sites in the interface which decrease the system energy, obtained by terminating carbon dangling bonds, indicated by open squares in the figure. (iii) Sites where in addition to the termination of dangling bonds, the existence of a hydrogen site causes a structural relaxation of the neighboring carbon atoms, and therefore the total system energy is lower than the dangling bond termination energy (these were indicated by the filled squares in the figure). Since the structural change between the ordered nano-diamond and disordered amorphous carbon in the interface causes a strain which increases the system energy, some of the hydrogen interstitial sites in the interface relax this strain and therefore reduce the system energy. A cubic spline interpolation calculation [26] has been made to interpolate between our data points.

We observe that on the diamond side of the interface region, there is a higher probability of finding sites with positive formation energy, where on the amorphous carbon side there are many sites with a negative formation energy, which is lower than the hydrogen formation energy in amorphous carbon.

## 5 Summary and conclusions

We deduce that

- The average hydrogen interstitial formation energy in the amorphous region is lower than the hydrogen interstitial formation energy in the nano-diamond. This difference increases when the hydrogen concentration in the nano-diamond core decreases. The formation energy difference is a driving force for the accumulation of hydrogen atoms in the amorphous region, adjacent to the nano-diamond core.
- There are several different types of sites in the interface between the amorphous carbon and the nano-diamond core, sites where the hydrogen atoms are not bonded and therefore have a positive formation energy, and sites where the hydrogen atoms terminate carbon dangling bonds and therefore have negative formation energies.
- The sites with a positive formation energy are on the nano-diamond core side of the interface, and may form a barrier for the diffusion of hydrogen atoms from the nano-diamond core to the amorphous region. The barrier height decreases with decreasing hydrogen concentration in the nano-diamond core.
- An energy well resulting from the high concentration of interstitial sites with a formation energy lower than the hydrogen interstitial formation energy in amorphous carbon is located at the amorphous layer side of the interface. Hydrogen atoms which accumulate in the interface between the nano-diamond core and the amorphous region are expected to be trapped in this well, and therefore reduce the structural strain of the interface. This conclusion is in agreement with our experimental results which show that hydrogen retention of diamond films increases with decreasing grain size, indicating the

likelihood that hydrogen is bonded and trapped in nano-diamond grain boundaries as well as on internal grain surfaces [6] see also ESR results of [46].

Our simulations suggest that hydrogen atoms are expected to be trapped in the interface between the nano-diamond core and the amorphous region and decorate the boundaries between a nano-diamond core and its surrounding amorphous shell. Invoking the eminently reasonable assumption that the amorphous shell models nano-diamond grain boundaries, our computational studies support our recent experimental results and conclusions.

## Acknowledgments

The calculations were carried out on the Computational Physics Group computers at the Technion. We thank Eduardo Warszawski for helpful discussions.

## References

- [1] Sh. Michaelson, O. Ternyak, A. Hoffman and Y. Lifshitz, Correlation between diamond grain size and hydrogen retention in diamond films studied by scanning electron microscopy and secondary ion mass spectroscopy, *Appl. Phys. Lett.*, 90 (2007), 031914.
- [2] Sh. Michaelson, O. Ternyak, R. Akhvlediani, O. A. Williams, D. Gruen and A. Hoffman, Hydrogen concentration and bonding in nano-diamond films of varying grain sizes grown by different chemical vapor deposition methods, *Phys. Stat. Sol.*, 204 (2007), 2860–2867.
- [3] Sh. Michaelson, O. Ternyak, R. Akhvlediani, A. Hoffman, A. Lafosse, R. Azria, O. A. Williams and D. M. Gruen, Hydrogen concentration and bonding configuration in polycrystalline diamond films: from micro-to nanometric grain size, *J. Appl. Phys.*, 102 (2007), 113516.
- [4] Y. Lifshitz, X. M. Meng, S. T. Lee, R. Akhvlediani and A. Hoffman, Visualization of diamond nucleation and growth from energetic species, *Phys. Rev. Lett.*, 93 (2004), 056101.
- [5] A. Hoffman, A. Heiman, R. Akhvlediani, E. Lakin, E. Zolotoyabko and C. Cytermann, Hydrogen content and density in nanocrystalline films of a predominant diamond character, *J. Appl. Phys.*, 94 (2003), 4589–4595.
- [6] Sh. Michaelson, O. Ternyak, A. Hoffman and Y. Lifshitz, Correlation between diamond grain size and hydrogen retention in diamond films studied by scanning electron microscopy and secondary ion mass spectroscopy, *Appl. Phys. Lett.*, 90 (2007), 031914.
- [7] A. Ito and H. Nakamura, Molecular dynamics simulation of bombardment of hydrogen atoms on graphite surface, *Commun. Comput. Phys.*, 4 (2008), 592–610.
- [8] Th. Frauenheim, F. Weich, Th. Kohler, S. Uhlmann, D. Porezag and G. Seifert, Density-functional-based construction of transferable nonorthogonal tight-binding potentials for Si and SiH, *Phys. Rev. B.*, 52 (1995), 11492–11501.
- [9] The Frauenheims Tight Binding (FTB) method is based on a second-order expansion of the Kohn-Sham total energy in density-functional theory [W. Kohn and L. J. Sham, *Phys. Rev.*, 140, (1965), A1133–A1138] with respect to charge density fluctuations. The zeroth order approach is equivalent to a common standard non-self-consistent tight-binding scheme, while at second order a transparent, parameter-free, and readily calculable expression for gener-

- alized Hamiltonian matrix elements is derived. The final approximate Kohn-Sham energy additionally includes a Coulomb interaction between charge fluctuations.
- [10] M. Elstner, D. Porezag, G. Jungnickel, J. Elsner, M. Haugk, Th. Frauenheim, S. Suhai and G. Seifert, Self-consistent-charge density-functional tight-binding method for simulations of complex materials properties, *Phys. Rev. B.*, 58 (1998), 7260–7268.
  - [11] W. Kohn and L. J. Sham, Self-consistent equations including exchange and correlation effects, *Phys. Rev.*, 140, (1965), A1133–A1138.
  - [12] R. Car and M. Parrinello, Unified approach for molecular dynamics and density-functional theory, *Phys. Rev. Lett.*, 55 (1985), 2471–2474.
  - [13] Th. Frauenheim, P. Blaudek, U. Stephan and G. Jungnickel, Atomic structure and physical properties of amorphous carbon and its hydrogenated analogs, *Phys. Rev. B.*, 48 (1993), 4823–4834; Th. Frauenheim, G. Jungnickel, Th. Kohler and U. Stephan, Structure and electronic properties of amorphous carbon: from semimetallic to insulating behaviour, *J. Non-Cryst. Solids.*, 182 (1992), 186–197.
  - [14] F. Stillinger and T. A. Weber, Computer simulation of local order in condensed phases of silicon, *Phys. Rev. B.*, 31 (1985), 5262–5271.
  - [15] A. S. Barnard and S. P. Russo, Development of an improved stillinger-weber potential for tetrahedral carbon using ab-initio (Hartree-Fock and MP2) methods, *Mol. Phys.*, 100(10) (2002), 1517–1525.
  - [16] A. Silverman, J. Adler and R. Weil, Computer modelling of the diffusion mechanisms of fluorine in amorphous silicon, *Thin. Solid. Films.*, 193/194 (1990), 571–576.
  - [17] Richard Zallen, *The Physics of Amorphous Solids*, Wiley-Interscience, New York, 1983.
  - [18] A. Sorkin, J. Adler and R. Kalish, Computer simulations of damage due to passage of a heavy fast ion through diamond, *Phys. Rev. B.*, 70 (2004), 064110.
  - [19] G. Kopidakis, I. N. Remediakis, M. G. Fyta and P. C. Kelires, Atomic and electronic structure of crystalline-amorphous carbon interfaces, *Diam. Relat. Mater.*, 16 (2007), 1875–1881.
  - [20] Sh. Michaelson, R. Akhvlediani, A. Hoffman, A. Silverman and J. Adler, Hydrogen in nano-diamond films: experimental and computational studies, *Phys. Stat. Sol.*, 205 (2008), 2099–2107.
  - [21] M. Parrinello and A. Rahman, Crystal structure and pair potentials: a molecular-dynamics study, *Phys. Rev. Lett.*, 45 (1980), 1196–1199.
  - [22] M. Parrinello and A. Rahman, A polymorphic transitions in single-crystals: a new molecular dynamics method, *J. Appl. Phys.*, 52 (1981), 7158.
  - [23] D. Saada, J. Adler and R. Kalish, Computer simulation of damage in diamond due to ion impact and its annealing, *Phys. Rev. B.*, 59 (1999), 6650–6660.
  - [24] A. P. Horsfield, Efficient ab initio tight binding, *Phys. Rev. B.*, 56 (1997), 6594–6602.
  - [25] A. P. Horsfield and A. M. Bratkovsky, Ab initio tight binding, *J. Phys. Condens. Mat.*, 12 (2000), R1.
  - [26] William H. Press, Saul A. Teukolsky, William T. Vetterling and Brian P. Flannery, *Numerical Recipes, The Art of Scientific Computing*, Cambridge University Press, 2007.
  - [27] J. Adler, J. Fox, R. Kalish, T. Mutat, A. Sorkin and E. Warszawski, The essential role of visualization for modeling nanotubes and nanodiamond, *Comput. Phys. Commun.*, 177 (2007), 19–20.
  - [28] Joachim Stohr, *NEXAFS Spectroscopy* (Springer Series in Surface Sciences), Springer, 2003.
  - [29] E. Warszawski, A. Hoffman, A. Silverman and J. Adler, Experiment (NEXAFS) versus simulation (DOS) for carbon allotropes, *Bulletin of the Israel Physical Society*, 52 (2006), 38; and to appear in *Computer Physics Communications*.

- [30] N. A. Marks, D. R. McKenzie, B. A. Pailthorpe, M. Bernasconi and M. Parrinello, Microscopic structure of tetrahedral amorphous carbon, *Phys. Rev. Lett.*, 76 (1996), 768–771.
- [31] N. A. Marks, D. R. McKenzie, B. A. Pailthorpe, M. Bernasconi and M. Parrinello, Ab initio simulations of tetrahedral amorphous carbon, *Phys. Rev. B.*, 54 (1996), 9703–9714.
- [32] D. G. McCulloch, D. R. McKenzie and C. M. Goringe, Ab initio simulations of the structure of amorphous carbon, *Phys. Rev. B.*, 61 (2000), 2349–2355.
- [33] A. Hoffman, M. Petracic, G. Comtet, A. Heurtel, L. Hellner and G. Dujardin, Photon-stimulated desorption of H<sup>+</sup> and H<sup>-</sup> ions from diamond surfaces: evidence for direct and indirect processes, *Phys. Rev. B.*, 59 (1999), 3203–3209.
- [34] D. Saada, J. Adler and R. Kalish, Lowest-energy site for hydrogen in diamond, *Phys. Rev. B.*, 61 (1999), 10711–10715.
- [35] J. P. Goss, R. Jones, M. I. Heggie, C. P. Ewels, P. R. Briddon and S. Oberg, First principles studies of H in diamond, *Phys. Stat. Sol. A.*, 186 (2001), 263–268.
- [36] J. P. Goss, R. Jones, M. I. Heggie, C. P. Ewels, P. R. Briddon and S. Oberg, Theory of hydrogen in diamond, *Phys. Rev. B.*, 65 (2002), 115207–115220.
- [37] M. Kaukonen, J. Peräjoki, R. M. Nieminen, G. Jungnickel and Th. Frauenheim, Locally activated monte carlo method for long-time-scale simulations, *Phys. Rev. B.*, 61 (2000), 980–987.
- [38] T. Nishimatsu, Ab initio study of donor-hydrogen complexes for low-resistivity n-type diamond semiconductor, *Jpn. J. Appl. Phys.*, 41 (2002), 1952–1962.
- [39] C. P. Herrero and R. Ramirez, Diffusion of muonium and hydrogen in diamond, *Phys. Rev. Lett.*, 99 (2007), 205504–205508.
- [40] P. Briddon, R. Jones and G. M. S. Lister, Hydrogen in diamond, *J. Phys. C.*, 21 (1988), L1027–L1031.
- [41] M. I. Heggie, C. P. Ewels, N. Martsinovich, S. Scarle, R. Jones, J. P. Goss, B. Hourahine and P. R. Briddon, Glide dislocations in diamond: first-principles calculations of similarities with and differences from silicon and the effects of hydrogen, *J. Phys. Cond. Matt.*, 14, (2002), 12689–12696; J. P. Goss, P. R. Briddon, S. J. Sque and R. Jones, Boron-hydrogen complexes in diamond, *Phys. Rev. B.*, 69 (2004), 165215–165223.
- [42] S. P. Mehandru, A. B. Anderson and J. C. Angus, Hydrogen binding and diffusion in diamond, *J. Mater. Res.*, 7 (1992), 689–695.
- [43] C. H. Chu and S. K. Estreicher, Similarities, differences, and trends in the properties of interstitial H in cubic C, Si, BN, BP, AlP, and SiC, *Phys. Rev. B.*, 42 (1990), 9486–9495.
- [44] N. M. J. Conway, A. Ilie, J. Robertson, W. I. Milne and A. Tagliaferro, Reduction in defect density by annealing in hydrogenated tetrahedral amorphous carbon, *Appl. Phys. Lett.*, 73 (1998), 2456–2459.
- [45] A. von Keudell, M. Meier and C. Hopf, Growth mechanism of amorphous hydrogenated carbon, *Diam. Relat. Mater.*, 11 (2002), 969–975.
- [46] D. F. Talbot-Ponsonby, M. E. Newton, J. M. Baker, G. A. Scarsbrook, R. S. Sussmann, A. J. Whitehead and S. Pfenninge, Multifrequency EPR, 1H ENDOR, and saturation recovery of paramagnetic defects in diamond films grown by chemical vapor deposition, *Phys. Rev. B.*, 57 (1998), 2264–2270.